CORA Cork Open Research Archive
Cartlann Taighde Oscailte Chorcaí

Title	Cobalt phosphate-based supercapattery as alternative power source for implantable medical devices
Authors	Shao, Han;Padmanathan, Narayanasamy;McNulty, David;O'Dwyer, Colm;Razeeb, Kafil M.
Publication date	2018-12-26
Original Citation	Shao, H., Padmanathan, N., McNulty, D., O'Dwyer, C. and Razeeb, K. M. (2019) 'Cobalt Phosphate-Based Supercapattery as Alternative Power Source for Implantable Medical Devices', ACS Applied Energy Materials, 2(1), pp. 569-578. doi: 10.1021/acsaem.8b01612
Type of publication	Article (peer-reviewed)
Link to publisher's version	https://pubs.acs.org/doi/10.1021/acsaem.8b01612 - 10.1021/acsaem.8b01612
Rights	© 2018 American Chemical Society. This article is made available for a limited time sponsored by ACS under the ACS Free to Read License, which permits copying and redistribution of the article for non-commercial scholarly purposes. - https://pubs.acs.org/page/policy/freetoread/index.html
Download date	2023-05-05 01:10:05
Item downloaded from	http://hdl.handle.net/10468/7270

UCC
University College Cork, Ireland
Coláiste na hOllscoile Corcaigh

This article is made available for a limited time sponsored by ACS under the ACS Free to Read License, which permits copying and redistribution of the article for non-commercial scholarly purposes.

ACS APPLIED ENERGY MATERIALS

Article

Cite This: ACS Appl. Energy Mater. 2019, 2, 569−578

www.acsaem.org

Cobalt Phosphate-Based Supercapattery as Alternative Power Source for Implantable Medical Devices

Han Shao,[†,‡] N. Padmanathan,[†] David McNulty,[‡] Colm O'Dwyer,[†,‡] and Kafil M. Razeeb*[,†]

[†]Micro-Nano Systems Centre, Tyndall National Institute, University College Cork, Dyke Parade, Lee Maltings, Cork T12 R5CP, Ireland

[‡]Department of Chemistry, University College Cork, Cork T12 YN60, Ireland

Supporting Information

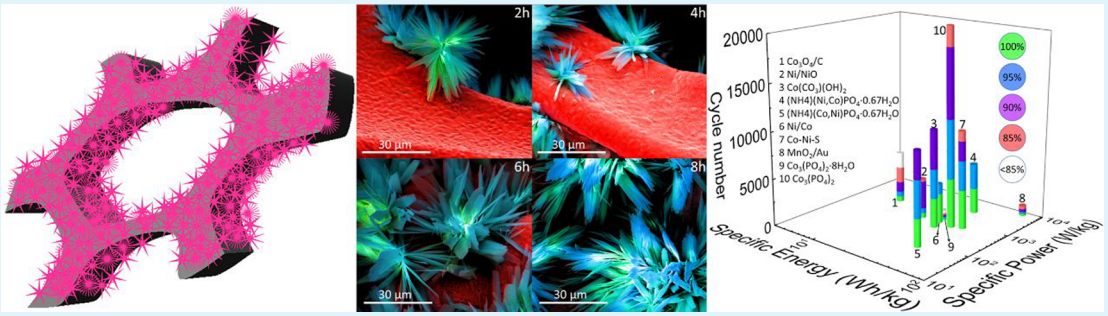

ABSTRACT: The supercapattery is an ideal energy storage device that combines excellent power density and rate capability of supercapacitors and the greater energy density of batteries. With superior storage capacity and long life, this device can be employed in next-generation artificial cardiac pacemakers as a rechargeable energy source for the lifetime of the pacemaker (at least 15−20 years). However, current hybrid energy storage devices are often limited by less than ideal performance of either the supercapacitor or battery. Here, we develop a low cost and scalable prototype supercapattery with cobalt phosphate as positive and activated carbon as negative electrodes. This positive electrode exhibits a maximum specific capacity of 215.6 mAh g^{-1} (≈1990 F g^{-1}), ever reported in a metal phosphate based electrode. The supercapattery delivers a high energy density of 3.53 mWh cm^{-3} (43.2 Wh kg^{-1}) and a power density of 425 mW cm^{-3} (5.8 kW kg^{-1}). Furthermore, the device can retain 79% voltage even after 4 min self-discharge, enough to provide power during cardiac emergencies. This hybrid device provides excellent performance and stability under physiological temperature range (35−41 °C), retaining 68% of specific capacity after 100 000 cycles at room temperature (25 °C) and up to 81.5% after 20 000 cycles at 38 °C, demonstrating its effectiveness as a potential power source for the next-generation implanted medical devices.

KEYWORDS: *cobalt phosphate, nanomaterial, supercapattery, supercapacitor, electrochemical, energy storage device*

INTRODUCTION

Implanted medical devices (IMDs), including implantable neurostimulators, artificial cardiac pacemakers, drug delivery systems, and insulin pumps, have drawn much attention in the scientific and medical industries.[1,2] These devices are currently powered by Li-ion batteries. The average pacemaker lithium ion battery has about 0.5−2 Ah of storage capacity[3] with an estimated operating life of around 6−11 years.[4] Recently, the Micra transcatheter pacing system has been developed with an expected battery longevity of 12 years.[5] However, in the development of implantable medical devices, in particular leadless devices, the power source cannot be replaced and should ideally last for 20 years or more.

Recently, silicon-based piezoelectric devices have been proposed to generate electrical power from the mechanical energy of heartbeats to operate the pacemaker,[6,7] where the electrical energy is stored using a battery to power the electronics of the pacemaker and to deliver the electrical impulses during a cardiac emergency (self-rechargeable pacemaker). However, the state of the art rechargeable Li-ion battery cyclability is limited to only 1500 cycles, which is far from the requirement of more than 10 years[4] lifetime (or at least 20 000 cycles) without loss of power. This then poses a significant issue for the long-term operation of the implanted medical device and the safety of the recipient.

Therefore, the development of a new type of energy storage device with enhanced cyclability and storage capacity is necessary for the next generation of leadless implantable medical devices. In addition, it will be necessary to considerably reduce the average size of the device and the power source with a cell voltage of 2.8 V for the next generation biomedical devices[2].

The supercapattery, combining the best properties of both batteries and supercapacitors, was proposed in 2011.[8] The

Received: September 24, 2018
Accepted: December 26, 2018
Published: December 26, 2018

Downloaded via UNIV COLG CORK on January 28, 2019 at 08:24:27 (UTC).
See https://pubs.acs.org/sharingguidelines for options on how to legitimately share published articles.

© 2018 American Chemical Society

DOI: 10.1021/acsaem.8b01612
ACS Appl. Energy Mater. 2019, 2, 569−578

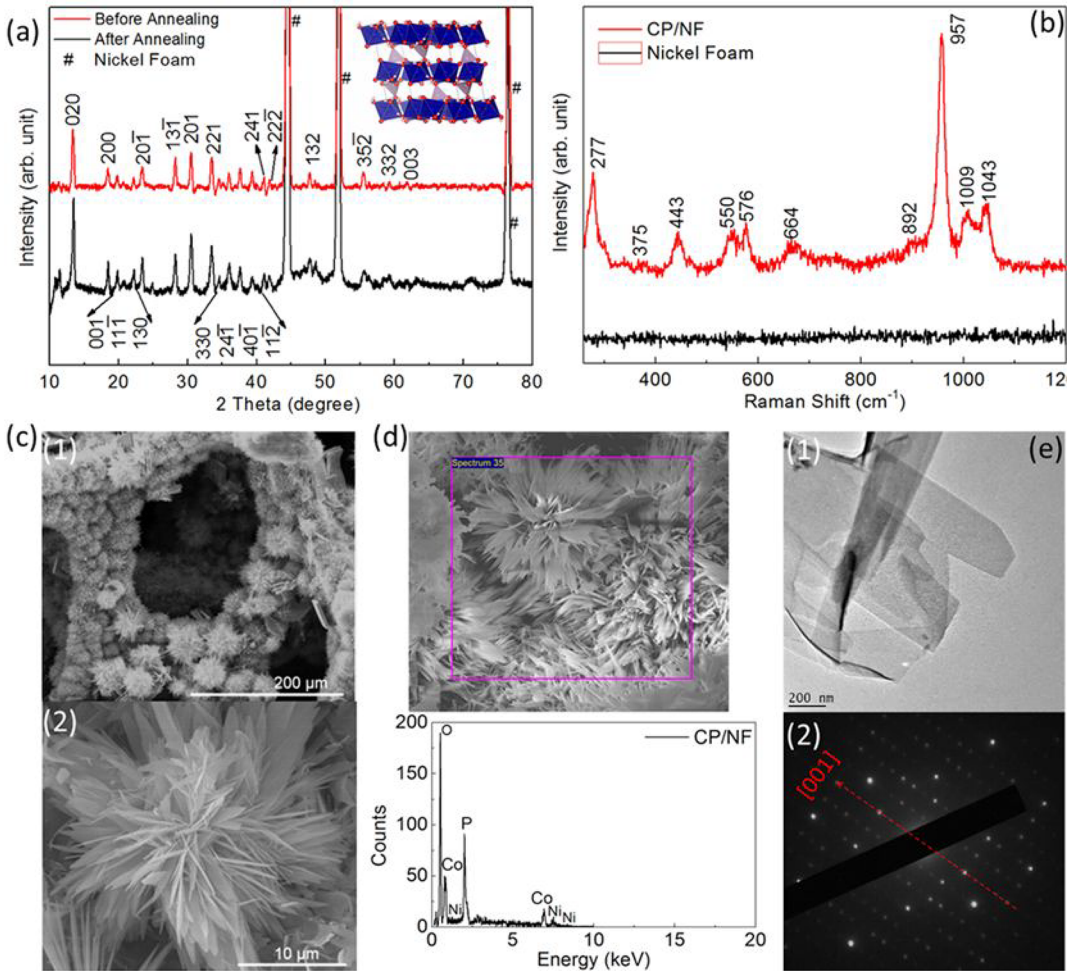

Figure 1. Material characterizations of cobalt phosphate electrode: (a) XRD patterns of cobalt phosphate electrode before and after annealing; (b) Raman spectra of cobalt phosphate electrode; (c) SEM images of cobalt phosphate electrode at different magnifications; (d) EDX analysis of cobalt phosphate electrode; (e) TEM image (1) and SAED pattern (2) of cobalt phosphate.

benefit of building a hybrid device is to obtain high energy from the battery-type material and coupling this with the ability to deliver high power from supercapacitor-type material. Due to the combination of two mechanisms, the supercapattery devices could potentially broaden the cell voltage and extend the cell lifetime[9,10] and is therefore particularly suited as an energy device for scalable and self-rechargeable leadless pacemakers. This has yet to be demonstrated, and this paper is the first work to demonstrate the potential for the supercapattery to be used in an implantable pacemaker.

Recent research efforts have been devoted to advance the electrode materials for supercapatteries, most often involving carbon materials,[11] metal oxides,[12,13] conducting polymers,[14] and in recent years metal−organic frameworks (MOFs).[15] Among them, transition metal oxides (TMOs), especially cobalt-based materials, have been widely investigated as the positive electrode for supercapatteries[12,16−18] owing to their multiple valence states available for redox processes and high theoretical capacity (275 mAh g^{-1}).[19] On the other hand, phosphate-based materials (Li(Fe, Mn)PO_4) have already been commercialized in battery manufacturing[20,21] due to their large discharge voltage window[22,23] and good stability at high temperature.[24] In terms of phosphate-based hybrid devices, a cobalt nickel phosphate[25−31] based device exhibited a reasonable specific energy of 45.8 Wh kg^{-1}, but the retention of the cell was only 57.8% after 2500 cycles, due to the dissolution of the active material during the electrochemical redox reaction.

In this paper, we report on the synthesis of cobalt phosphate nano-/microstructure via hydrothermal method as supercapattery electrode for next generation leadless pacemaker. The device should work effectively, steadily, and safely inside the human body for at least 15−20 years, which requires the nano-/microstructure to offer high capacity (capacitance) and excellent stability. Furthermore, an investigation on the thermal stability of the device under physiological temperature range is also necessary. The electrochemical performance variation, self-discharge behavior, and cyclic stability under a temperature range of 25−45 °C have to be controlled in an acceptable range. Thus, our study is focused on the fabrication of nanoflakes/microflower cobalt phosphate based supercapattery and detail investigation on the mechanism, structure, and electrochemical properties, which showed outstanding electrochemical performance and could be a promising alternative power source to replace the battery in the next generation self-rechargeable pacemaker and relative implantable biomedical devices.

DOI: 10.1021/acsaem.8b01612
ACS Appl. Energy Mater. 2019, 2, 569−578

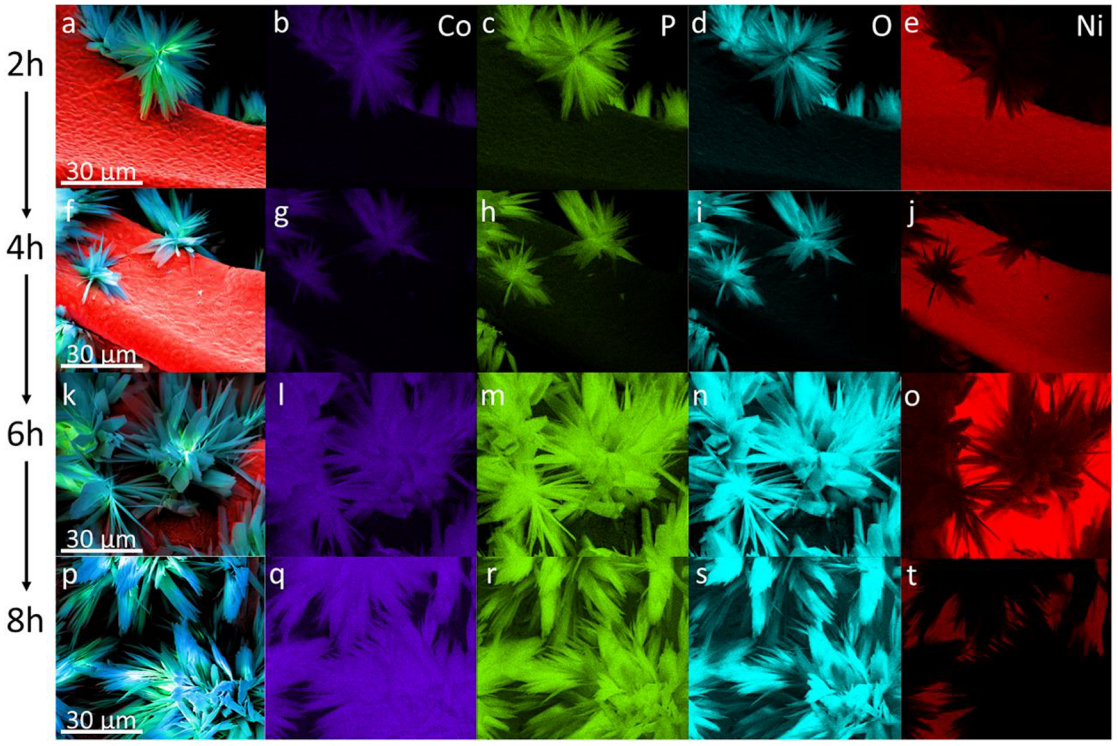

Figure 2. Growth process identification by EDX mapping: (a) phase distinguishable elemental mapping for 2 h sample; (b–e) EDX elemental mapping for Co, P, O, Ni elements. Parts f–j, k–o, and p–t are corresponding results for 4, 6, and 8 h samples, respectively.

EXPERIMENTAL PROCEDURES

Material Synthesis. $Co_3(PO_4)_2$/Nickel Foam (CP/NF) Electrode. $Co_3(PO_4)_2$ nanoflakes/flower was grown over nickel foam (NF) (Changsha Lyrun New Materials Co., LTD, China, porosity 95%) via hydrothermal method. More specifically, nickel foam (3 × 3 cm^2) was treated in 3 M HCl (Sigma-Aldrich, ACS reagent) with ultrasonication for 10 min, followed by washing with ethanol and deionized water for 15 min, then dried overnight to be used as substrate. 2.5 mM $Co(NO_3)_2{\cdot}6H_2O$ (Sigma-Aldrich, ACS reagent) and 2.5 mM $NH_4H_2PO_4$ (Sigma-Aldrich, 99.999% trace metals basis) were dissolved in the deionized (DI) water under stirring for 15 min to form the transparent light pink solution. The pretreated nickel foam and light pink solution were transferred to a 100 mL autoclave and then kept at 120 °C for 8 h in an oven. After cooling down to the room temperature naturally, the sample was washed with DI water, ethanol, and acetone with the assistance of ultrasonication three times. After drying, the sample was annealed at 120 °C for 12 h in the oven. The loading mass of the $Co_3(PO_4)_2$ nanoflakes/flower was calculated by subtracting the weight of pure nickel foam from the weight of nickel foam with $Co_3(PO_4)_2$ after the growth process. Typical mass of $Co_3(PO_4)_2$ nanoflakes/flower was ~4.5 mg/cm^2. Figure S1 in Supporting Information shows a photograph of $Co_3(PO_4)_2{\cdot}8H_2O$/NF samples before (pink-purple color) and after (purple color) annealing.

Activated Carbon/Nickel Foam (AC/NF) Electrode. The activated carbon-based electrode was prepared by spreading the mixture of activated carbon (Sigma-Aldrich, Analytical reagent) (75 wt %), super P (Imerys Graphite & Carbon Belgium SA, Belgium, carbon black >96%) (15 wt %) and PVDF (polyvinylidene difluoride) (Sigma-Aldrich, average M_w ~ 534 000) (10 wt %) on 3 M HCl pretreated nickel foam. Typical mass loading of AC/NF electrode was ~12 mg/cm^2.

Material Characterization. The crystal structures of CP/NF samples were analyzed using X-ray diffractometer (XRD Philips PW3710-MPD diffractometer with Cu Kα radiation, λ = 1.54 Å). The surface morphology and compositional analysis of CP/NF samples were performed by field emission scanning electron microscope (FEI QUANTA 650 HRSEM) with an energy dispersive X-ray spectroscopy (EDX Oxford Instruments INCA energy system) and high resolution transmission electron microscope (JEOL HRTEM-2100 at 200 kV). To avoid contribution of Ni from the nickel foam (NF), the EDX and TEM measurements were carried out for the powder samples scratched off from the NF. The Raman spectra of CP/NF hybrid structures were recorded with the Renishaw (RA 100) in Via confocal Raman microscope at 514.5 nm excitation. The X-ray photoelectron spectroscopy (XPS) analysis was performed on a Kratos Ultra DLD spectrometer with Al K α (1486.6 eV) as the X-ray source

Electrochemical Measurements. The electrochemical performance of the CP/NF electrodes was investigated in a three-electrode system using platinum wire (Pt) and saturated calomel electrode (SCE) as counter and reference electrodes, respectively. The electrolyte was 3 M KOH solution. The electrochemical properties of hybrid cell were evaluated in a two-electrode system using CP/NF as positive electrode and AC/NF as negative electrode separated by Celgard separator (50% porosity) in 3 M KOH (J. T. Baker, ACS reagent) solution. Both positive and negative electrodes were cut into 1 × 1 cm^2 and then assembled into a supercapattery. Further details are found in the Supporting Information. In order to investigate the electrochemical properties of the device inside the human body, further study of the device was carried out at temperatures ranging from 25 to 45 °C. The electrochemical measurements, including cyclic voltammetry (CV), chronopotentiometry, and ac impedance techniques, were conducted using a Biologic VSP Modular 5 channels potentiostat.

RESULTS AND DISCUSSION

Structure and Morphology Characterization. The crystal structure and phase of nickel foam-supported cobalt phosphate was determined by XRD before and after annealing as shown in Figure 1a. Both samples can be indexed to cobalt phosphate hydrate (JCPDS 33-0432) with monoclinic crystal structure. After dehydrating at 120 °C for 12 h, the electrode color changed from pink-purple to purple, (Figure S1 in

DOI: 10.1021/acsaem.8b01612
ACS Appl. Energy Mater. 2019, 2, 569–578

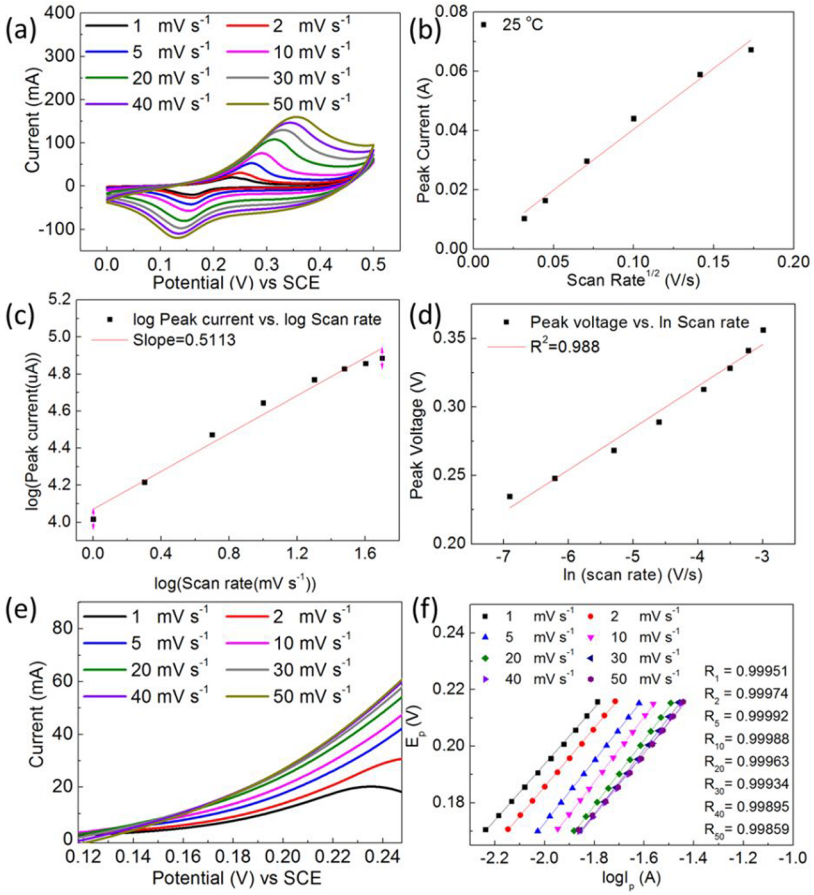

Figure 3. (a) Cycle voltammograms, (b) plot of forward anodic peak current density and the square root of the scan rate, (c) plot of log peak currents (I_{pa}) against the log scan rate (ν), (d) plot of peak voltage vs ln scan rate for CP/NF in three electrode system, (e) raising part of CV curve of the cobalt phosphate electrode at different scan rates and the corresponding Tafel plot (f).

Supporting Information), which may be associated with the loss of surface water during annealing. However, reflections from the planes of cobalt phosphate became narrow and intense, which indicates that the low temperature annealing process enhanced the crystal quality.[10]

The observed room temperature Raman spectra in Figure 1b further support the growth of high quality cobalt phosphate hydrate structure on NF. The peak at 277 cm^{-1} is due to the O−Co−O bending,[26] and the high intensity peak at 957 cm^{-1} assigned to the v1 PO_4^{-3} symmetric stretching vibrations,[26,27] the peaks at 1009 and 1043 cm^{-1} are assigned to v3 PO_4^{-3} asymmetric stretching modes.[27,28] The low intensity peak at 664 cm^{-1} corresponds to the v4 bending of the PO_4^{-3} unit. The O−P−O and P−O−P bending modes are located at 443 and 894 cm^{-1},[27,29] respectively. Raman bands at 550 and 576 cm^{-1} are attributed to the v2 PO_4 and H_2PO_4 bending modes.[32] All these Raman modes apparently confirm the formation of cobalt phosphate hydrate structure and corroborate with the XRD analysis.[26−28,33,34]

The low magnification SEM image in Figure 1c1 shows a homogeneous distribution of the cobalt phosphate nano/microflower over the nickel foam. Figure 1c2 confirms the cobalt phosphate nanoflake (with an average thickness from 100 to 400 nm) outward growth in different directions, forming a flower-like microstructure. The EDX (Figure 1d) and XPS (Figure S3) analyses clearly indicate the presence of the valence states of the Co, P, and O elements in cobalt phosphate sample. In addition, Figure 1e shows the TEM image of cobalt phosphate powder, which has been scratched off from the nickel foam. Figure 1e1 shows the substrate-delaminated few-nanoflake structures with an average thickness of 200 nm. Corresponding selected area electron diffraction (SAED) pattern in Figure 1e2 indicates good crystallinity of the multilayer structure of the cobalt phosphate nanoflakes and may be described as Bernal stacked single molecule layers with [001] growth direction.[35]

To comprehend the growth of nano-/microflower structure, time dependent experiment was performed and analyzed with SEM and EDX (see Figure 2 and section A in Supporting Information). In summary, cobalt phosphate nucleated on the nickel foam and grew in different directions to form the flower, which started to grow initially at the edges of the NF and then further grew toward the center. The detailed growth mechanism of the cobalt phosphate is discussed in section A of the Supporting Information.

Electrochemical Characterization. The electrochemical properties of the CP/NF nanoflakes/microflower structure were investigated using a three electrode system. In order to exclude the contribution of nickel foam substrate, cyclic voltammograms (CV) and charge−discharge studies were carried out for the NF and CP/NF as shown in parts a and b of Figure S4. The capacity of NF and CP/NF was found to be 0.023 and 0.970 mAh cm^{-2}, which indicates that cobalt phosphate is the principal contributor to the charge storage of the electrode. Figure 3a shows the CV curves of CP/NF at different scan rates from 1 to 50 mV s^{-1}. The pair of oxidation

DOI: 10.1021/acsaem.8b01612
ACS Appl. Energy Mater. 2019, 2, 569−578

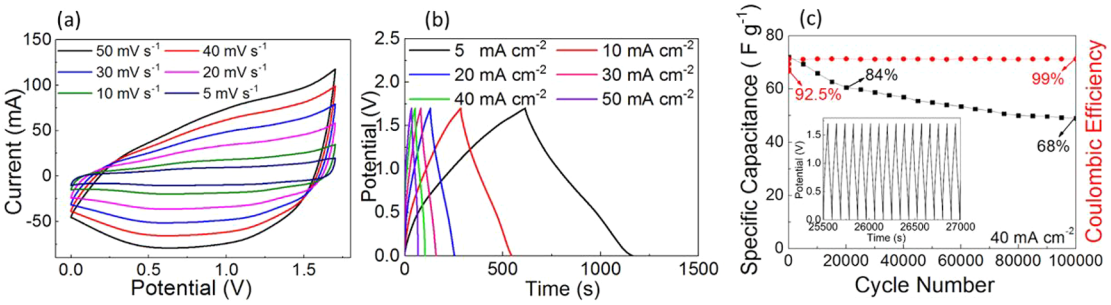

Figure 4. Electrochemical and cycle-life profiling of the supercapattery: (a) cycle voltammograms, (b) charge−discharge profiles, and (c) cyclic stability of the CP/NF//AC/NF supercapattery with charge−discharge curves as shown in the inset.

and reduction peaks indicate the faradaic energy storage mechanism of the electrode material. With faster scan rate the peak separation increased, representing quasi-reversible faradaic reaction on the electrode surface.

The observed peak currents (I_{pa}) are proportional to the square root of the scan rate (ν) (as shown in Figure 3b, measured at 25 °C with the equation of $I_{pa}(A) = 0.3518\sqrt{\nu\ (\mathrm{V/s})} + 0.00369$ and $R^2 = 0.9862$. Thereby, it can be realized that the process is diffusion-controlled process rather than surface-controlled process. From the theoretical point of view, a slope of 0.5 or 1.0 is expected for the plot of log I_{pa} vs log ν under diffusion or adsorption-controlled process, respectively.[36] As can be observed, a linear curve was shown in the lot of log I_{pa} vs log ν (Figure 3c) with a slope of 0.5113, which is close to the theoretically predicted value of 0.5 for a purely diffusion-controlled process.[36] Furthermore, the plot of peak voltage vs ln ν shows a linear behavior (Figure 3d), which confirms the diffusion-limited transfer process.

The peak shifting (1 mV/s vs 50 mV/s) for the oxidation peaks (121 mV) is larger than the reduction peaks (29 mV), which may be due to the quasi reversible oxidation and reduction of $Co^{2+} \leftrightarrow Co^{3+/4+}$. In general, OH^- ions are adsorbed upon oxidation and expelled during reduction, and thereby it is observed that the hydroxide ions are the dominant mobile species. Quasi or nearly symmetric nature of the CV curves at each scan rate indicates the good redox property of the material. The faradaic reactions in the overall process are[37,38]

$$Co_3(PO_4)_2 + OH^- \leftrightarrow Co_3(PO_4)_2(OH) + e^- \quad (1)$$

$$Co_3(PO_4)_2(OH) + OH^- \leftrightarrow Co_3(PO_4)_2(O) + H_2O + e^- \quad (2)$$

$$O + O \leftrightarrow O_2\uparrow \quad (3)$$

The electrochemical redox reaction mechanism was further supported by the Tafel equation:[39]

$$b = 2.303\frac{RT}{\alpha nF} \quad (4)$$

where b is Tafel slope, obtained from the Tafel plot (log I_p vs E_p) as shown in Figure 3e,f, α is charge transfer coefficient, n is electron transfer number, F is Faraday constant (96 485 C mol^{-1}), R is gas constant (8.314 J mol^{-1} K^{-1}), and T is temperature (298 K). α is often around 0.5, which is equal proportional of electrical energy for favoring forward reaction and suppressing the reverse reaction,[39] and then the electron transfer number is estimated to be 1.2, which indicated Co^{2+} had been oxidized to Co^{3+} and Co^{4+}. Furthermore, the diffusion coefficient was calculated using the Randles−Sevcik equation:[40]

$$I_p = (2.687 \times 10^5)n^{3/2}A\sqrt{D}\ C\sqrt{\nu} \quad (5)$$

where n is electron transfer number, A is the working area of the electrode (cm^2), C is the concentration (mol), D is the diffusion coefficient (cm^2 s^{-1}), and ν is the scan rate (mV s^{-1}). The calculated diffusion coefficient is 1.1×10^{-13}, further confirming hydroxide ions are the dominant mobile species.

Figure S5a shows the charge−discharge profile of the CP/NF at different applied current from 5 to 50 mA cm^{-2}. The quasi-reversible curves with distinct potential plateaus demonstrate the battery-type redox reaction on the electrode surface. The nearly symmetric charge−discharge curves at wide range of specific current indicate quasi reversible faradaic reaction of the electrode. At a high current, the cation mobility is enhanced by the interlayer gallery spacing between the lamellar sheets of $Co_3(PO_4)_2$ on the porous Ni foam current collector, which prevents significant ohmic drop (<0.7 mV) in the electrolyte and results in the high electrochemical activity.

Due to the typical faradaic charge compensation, the specific capacity was calculated using $C = It/m$, where I is applied current, t is discharge time, and m is the mass of the active material. A maximum specific capacity was found to be 215.6 mAh g^{-1} at an applied current of 5 mA. The value was reduced to 124.6 mAh g^{-1} at a higher current of 50 mA showing a capacity retention of 57.8% of the initial value with a 10-fold increase in applied current.

The word "pseudocapacitance" is used to describe those electrode materials that demonstrate a linear dependence of electrochemical charge storage properties like carbon based capacitor but with faradaic chemical reaction.[8,41−43] However, due to the misconception in the literature of the term "pseudocapacitance", many researchers have classified their materials with a behavior of a noticeably discharge plateau to be capacitive[43,44] and used the same equation to estimate the charge storage capacity. In order to compare with those results, the specific capacitance ($C = It/mV$) was calculated for our electrode, which showed a maximum capacitance of 1990 F g^{-1} at a current of 5 mA, which is much higher than the state of the art (1578.7 F g^{-1})[10] cobalt phosphate electrode and other metal phosphate based materials.[45−47] This may due to the 3D network architecture along with the thin nanoflakes offered the large contact area with electrolyte for more efficient ion and charge transport. Also the interconnected nanoflakes provided lots of nano-/microscale gaps, which were favorable for electrolyte penetration to the interior surfaces of the electrode. The stability of cobalt phosphate electrode was tested with a

DOI: 10.1021/acsaem.8b01612
ACS Appl. Energy Mater. 2019, 2, 569−578

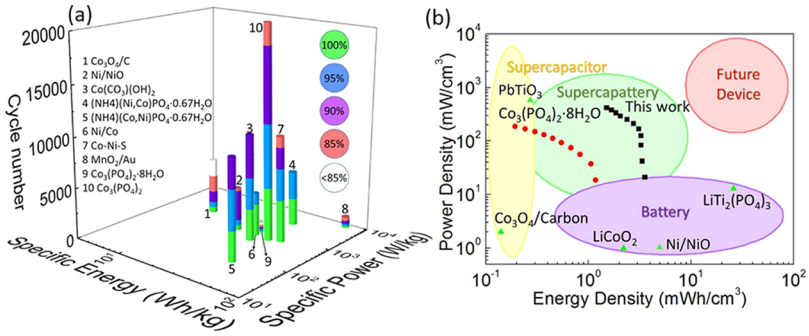

Figure 5. Supercapattery performance. (a) 3D gravimetric Ragone plots of the supercapattery and comparison with other works. The *z*-axis indicates the charge−discharge cycles reported for each device and the color-gradient map.[9,10,12,16,17,45,52,54,55] (b) Volumetric Ragone plots of the CP/NF//AC/NF supercapattery and comparison with other energy devices.[12,53,56−58]

continuous charge−discharge cycles at a specific current of 40 mA as shown in Figure S5b. The interconnected nanoflakes provided a rigid structure so that the electrode showed an excellent stability of 90.5% after the first 5000 cycles and retains 80.4% of its initial capacity after 20 000 cycles. These results are much better than the reported cobalt[12,17] and phosphate[45,48,49] based electrodes in terms of capacitance (up to 1492 F g^{-1}) and cyclability (up to 10 000 cycles).

Supercapattery Performance. Considering the outstanding electrochemical activity of cobalt phosphate on nickel foam, we fabricated a supercapattery (Figure S6) using the CP/NF as positive electrode and activated carbon on nickel foam (AC/NF) as negative electrode and tested in 3.0 M KOH solution. Figure S7 in Supporting Information depicts the individual CV curves of positive and negative electrodes, where the CP/NF shows a noncapacitive faradaic mechanism in the potential range 0−0.5 V. The AC/NF electrode demonstrated a typical capacitive behavior between −1.0 and 0.2 V, due to physical electrostatic adsorption of ions at the interface between electrode and electrolyte. Thereby, a large potential window of 1.7 V was obtained in the supercapattery as shown in Figure 4a. Due to the combination of two different charge storage mechanisms, the CV response shows quasi-rectangular shape at low scan rate and further shape deviation at higher scan rate. This may be due to the electron/ion transport restricted to certain limit on the electrode surface at high scan rate (current flowing) during the redox process.

Figure 4b shows the charge−discharge curves of the supercapattery at different applied currents. Quasi-linear charge−discharge curves confirm both the capacitive and battery-like characteristic of the device, which is in good agreement with the CV analysis. A maximum specific capacity of 50.84 mAh g^{-1} (capacitance 107.7 F g^{-1}) at an applied current of 5 mA is observed, using the active materials' weight of the device. Increasing the applied current by an order of magnitude (up to 50 mA) decreased the capacity to 30.71 mAh g^{-1}(capacitance 65.0 F g^{-1}). Even at a high current of 100 mA, the capacity remained stable at 24.26 mAh g^{-1}, which is 47.7% of the initial value for 20× the initial current. Due to the nonlinear charge−discharge behavior, the specific energy and power were calculated according to $E = I\int_{t=0}^{t=t} V(t)\,dt$ and $P = E/t$. A maximum energy density of 3.53 mWh cm^{-3} (43.2 Wh kg^{-1}) was observed at a specific power of 8.5 mW cm^{-3} (293.1 W kg^{-1}), which is nearly 50% of the lithium iron phosphate based battery (90−110 Wh kg^{-1}).[50] Even at a high current of 100 mA, the energy density remains at 1.49 mWh cm^{-3} (20.6 Wh kg^{-1}) and reached a peak power density of 425 mW cm^{-3} (5.8 kW kg^{-1}), which is similar to the maximum specific energy reported for most cobalt based devices.[12,16,17]

To replace the pacemaker battery system with this supercapattery, its storage performance must be comparable with the battery in an actual pacemaker. Assuming the pacemaker has to deliver 10 (usually it is twice per day for the pacemaker battery life estimation)[4] impulses per day, then for 20 years lifetime the device has to be operational for at least 73 000 charge−discharge cycles. Thereby, we investigated 100 000 cycles at a charge−discharge current of 40 mA for our hybrid device. We observed no loss after 2000 cycles (100% retention capability), and the device suffered just a 9.5% capacity loss after 10 000 cycles and retained 84% of the initial value (Figure 4c) after 20 000 cycles. Surprisingly, after 100 000 cycles, the capacity dropped to 68%, while the voltage remained at 1.5 V which confirms excellent cyclability of the device. The shelf life of a lithium battery is typically equivalent to 90% capacity retention over 5 years.[4] With similar retention, our hybrid device survived 10 000 cycles, which means 14 years of operability, according to two pulses delivered per day for the pacemaker battery life estimation.[4] Furthermore, a battery is determined to be invalid when its capacity retention is below 80%.[51] Our device can retain 84% capacity over 20 000 cycles and thereby can be active for more than 24 years (at two pulses per day), meeting the stringent requirement of the pacemaker (20 years lifetime).

The Coulombic efficiency of the device was calculated to be 92.5%, 93.5%, 96.2% for the 10th, 20th, 30th cycles, and this may be due to the formation of solid electrolyte interphase. After 100 charge−discharge cycles, the Coulombic efficiency is ∼99% and quite stable (Figure 4c), indicating the redox process repeats in a consistent manner. SEM and EDX analysis (Figure S8 in Supporting Information) of cobalt phosphate electrode after 20 000 cycles showed no major change in nanoflakes/microflower structure aside from some granular particles, likely due to the partial dissolution (0.15 mg loss) of the active material. The formation of potassium cobalt phosphate at the electrode surface after 100 000 cycles and the more granular morphology are confirmed by the SEM, EDX (Figure S9 in Supporting Information) and XRD analysis (Figure S10 in Supporting Information).

The 3D Ragone plot of Figure 5a compares our supercapattery with state of the art metal oxide and phosphate based devices and displays the retention of the initial capacitance/capacity after certain numbers of cycles from green (100%), blue (95%), purple (90%), and pink (85%) to white (<85%).

DOI: 10.1021/acsaem.8b01612
ACS Appl. Energy Mater. 2019, 2, 569−578

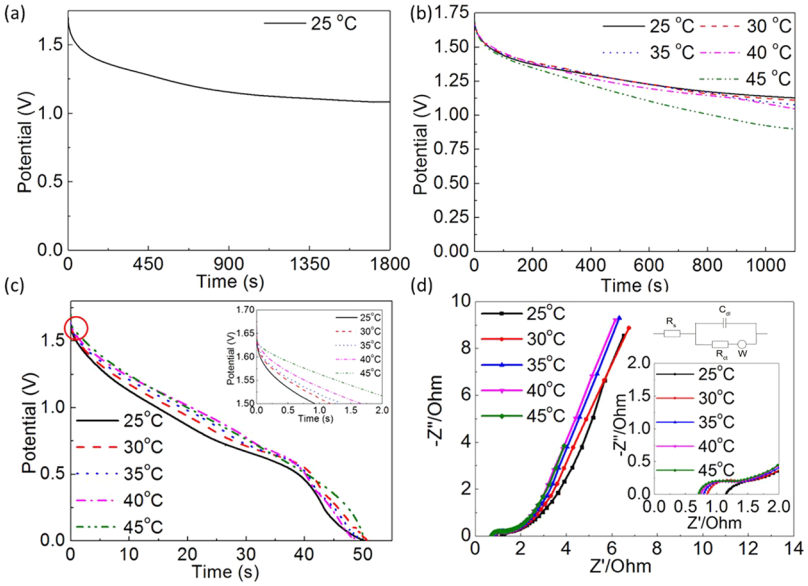

Figure 6. Monitoring self-discharge of pacemaker supercapattery: (a) self-discharge curves of supercapattery at different temperature from 25 to 45 °C; (b) plot of forward anodic peak current density and the square root of the scan rate for CP/NF at different temperature from 25 to 45 °C in three electrode system; (c, d) discharge curve (at 40 mA/cm^2) (inset showing magnified view of the graph for first 2 s) and Nyquist plots (with equivalent circuit and magnified view of the graph as insets) of the hybrid device at different temperature from 25 to 45 °C.

Obviously, the MnO_2/Au based device achieved a high specific energy of 57 Wh kg^{-1} but only survives 1000 cycles with a decay of 15%.[52] Among all the cobalt and phosphate based devices summarized in Figure 5a, our supercapattery shows the best specific energy with beyond state of the art cyclability. In terms of volumetric density (Figure 5b), $LiTi_2(PO_4)_3$ based batteries[53] can obtain a high energy density of 26−31 mWh cm^{-3}; however, the retention is limited to 2000 cycles. Our device exhibits a higher power density than other battery/supercapattery devices with an acceptable energy density. The space allocated (5 mm inner diameter × 13 mm height) for the energy storage device can accommodate six layers of supercapattery cells (5 mm × 2 mm) connected in series and should be able to store 0.175 mWh energy and deliver 49.98 mW (equivalent to 49.98 mJ/s) power, which is nearly 2000 times the pacemaker pulse requirements of 25 μJ.[4] In order to demonstrate the usability of the device, two supercapatteries were connected in series to power an LED. By charging the devices through a USB port for 1 min, the LED remained lit for up to 20 min with no loss in brightness in the first minute as shown in Figure S11and in the video. Even after 5000 charge−discharge cycles, the devices were still capable of powering the LED with similar brightness to the initial test, which confirms the long-term usability of the proposed supercapattery device.

Self-Discharge Avoidance in Pacemaker Supercapattery. To ensure that a pacemaker retains enough energy to provide electrical impulses during emergency, the self-discharge behavior and leakage current of CP/NF//AC/NF supercapattery device were investigated by measuring the open-circuit voltage, immediately after the device was fully charged with a charging current of 5 mA, as shown in Figure 6a. The self-discharge is mainly due to the migration of active electrolyte between two electrodes and the faradaic redox reaction from some depolarizing impurity.[59] The oxidation and reduction reaction, if it occurs on the surface of either electrode, could cause a voltage leak. Since clinical brain death occurs from oxygen starvation in 4 min after the heart stops beating, a supercapattery such as that developed in this work remains at 1.35 V (79.4% of the fully charged voltage) after 237 s, indicating that the device can provide enough power during cardiac emergencies. In addition, the device maintained more than 66% of the initial voltage after 1100 s and remains stable for another 700 s.

Operation under Physiological Conditions (25−45 °C). For use under physiological conditions inside the human body, studies on the electrochemical properties were carried out between 25 and 45 °C.[60] Besides the electrochemical properties and purity of the reagents, temperature is another important factor that determines the self-discharge current ($I = A \exp\left[-\frac{\Delta E^+}{RT}\right]$, where ΔE is a positive quantity around 16−20 kJ mol^{-1} for diffusion controlled reactions).[59] As shown in Figure 6b, the leakage current of the device increases noticeably with increasing temperature, indicating the enhanced mobility of the electrolyte ions.

In order to understand the mechanism, individual electrodes (CP/NF and AC/NF) were investigated between 25 and 45 °C. For individual electrodes in a three-electrode system, the diffusion coefficient (Figure S12 slopes) is amplified with increasing the temperature, showing slightly improved activation energy. Thereby, in the case of the complete hybrid device (Figure 6c), it is observed a slight increase in specific capacity (from 29.51 to 34.88 mAh g^{-1}) due to the thermal activation of the electrode material. As presented in the Figure 6c inset, the *IR* drop decreased from 0.079 to 0.034 V for 25 to 45 °C, indicating slight decrease of the device resistance. From the Nyquist plots (Figure 6d) acquired in 5 °C increments from 25 to 45 °C, it is evident that the device behaves like an ideal supercapacitor in the low frequency region with a near-linear plot and an irregular semicircle was found at high frequency region. The diameter of the semicircle reflected the charge-transfer resistance (R_{ct}) process on the surfaces of electroactive materials and was caused by faradaic reactions. The straight line corresponds to Warburg impedance, which was related to the diffusion of the electroactive species,

DOI: 10.1021/acsaem.8b01612
ACS Appl. Energy Mater. 2019, 2, 569−578

indicating ion diffusion resistance. The resistance of the device was found to be 1.13−0.70 Ω, which is consistent with the discharge behavior and leakage current. Overall, the device is very stable and its capacity and voltage stability are within operational and safety norms for pacemaker power sources under nominal human body temperature (25−45 °C).

In addition, a charge−discharge study for 20 000 cycles at 38 °C showed only 18.5% decay in the initial capacity, similar to room temperature, indicating excellent electrochemical properties and stability for our cobalt phosphate based supercapattery for the pacemaker implanted inside the human body. This rechargeable supercapattery with a high energy density of 3.53 mWh cm^{-3} (43.2 Wh kg^{-1}) and retention of 68% after 100 000 cycles should be able to power the pacemaker for 20 years. The devices with single cell voltage of 1.7 V can be connected in series to meet the requirement of 2.8 V and would hold enough voltage (1.35 V) after the first 4 min with minimal self-discharge, which should be sufficient time for a piezoelectric energy harvester to recharge the device completely. The device exhibited good electrochemical properties at normothermia (38 °C) so that it is a promising forerunner for the development of a long-life rechargeable energy source for powering and operating next-generation self-charging pacemakers in conjunction with suitable energy harvesting technology.

CONCLUSIONS

In summary, we developed a cobalt phosphate-nickel foam nanoflakes/microflower structure electrode for supercapatteries and showed a high capacity of 215.6 mAh g^{-1} (equivalent to a capacitance of 1990 F g^{-1}), which decayed only 19.5% after 20 000 cycles. A fabricated supercapattery based on cobalt phosphate and activated carbon electrodes exhibited a high energy density of 3.53 mWh cm^{-3} (43.2 Wh kg^{-1}) and remained at 1.49 mWh cm^{-3} (20.6 Wh kg^{-1}) at a high power density of 425 mW cm^{-3} (5.8 kW kg^{-1}). The device demonstrated an excellent cyclability of 84% after 20 000 cycles, and even after 100 000 cycles, the capacitance dropped to 68% of the initial value, confirming a long-time reliability of our device. Furthermore, the cobalt phosphate based supercapattery is stable at room temperature and above body temperature (25−45 °C). The energy and power performance of this hybrid device exceed the stringent requirements of a leadless pacemaker system. Furthermore, in terms of power delivery, cycle life, self-discharge stability, and compatibility with human body temperature, our device exhibits state of the art performance. This relatively simple technology is being developed as a long-life rechargeable energy source for powering and operating next-generation self-charging pacemakers in conjunction with suitable energy harvesting technology. With further biological evaluation and device miniaturization, the concept of a higher energy density, fast charging power source for cardiac care in patients will be accomplished. This device is also adaptable to a range of other implanted medical devices and for Internet of Things (IoT) applications requiring rechargeable power sources for wireless sensor nodes.

ASSOCIATED CONTENT

Supporting Information

The Supporting Information is available free of charge on the ACS Publications website at DOI: 10.1021/acsaem.8b01612.

Digital photograph of $Co_3(PO_4)_2$ grown on NF substrate before and after annealing; growth mechanism of cobalt phosphate; XPS study on cobalt phosphate; cobalt phosphate electrochemical data in three electrode system; supercapattery device electrochemical data; SEM and XRD data for cyclability study; devices application; electrode electrochemical data under physiological conditions; comparison of electrochemical performance for different metal phosphate based electrode in three electrode configuration (PDF)

Video showing supercapatteries connected in series to power an LED (MP4)

AUTHOR INFORMATION

Corresponding Author

*Phone: +353 21 2346078. E-mail: kafil.mahmood@tyndall.ie.

ORCID

David McNulty: 0000-0002-6337-3395
Colm O'Dwyer: 0000-0001-7429-015X
Kafil M. Razeeb: 0000-0001-9360-9277

Funding

The authors acknowledge financial support from EU FP7 Project Manpower (Contract 604360) to carry out this work. We acknowledge support from Science Foundation Ireland under a Technology Innovation and Development Award (Grant 14/TIDA/2455)

Notes

The authors declare no competing financial interest.

REFERENCES

(1) Halperin, D.; Heydt-Benjamin, T. S.; Fu, K.; Kohno, T.; Maisel, W. H. J. I. p. c. Security and Privacy for Implantable Medical devices. *IEEE Pervasive Computing* **2008**, *7*, 30−39.

(2) Amar, A. B.; Kouki, A. B.; Cao, H. J. S. Power Approaches for Implantable Medical Devices. *Sensors* **2015**, *15*, 28889−28914.

(3) Shepard, R. K.; Ellenbogen, K. A. Leads and longevity: How Long Will Your Pacemaker Last? *Eur. Heart Rhythm Assoc.* **2008**, *11*, 142−143.

(4) Mallela, V. S.; Ilankumaran, V.; Rao, S. N. Trends in cardiac pacemaker batteries. *Indian Pacing Electrophysiol. J.* **2004**, *4*, 201−212.

(5) Reynolds, D.; Duray, G. Z.; Omar, R.; Soejima, K.; Neuzil, P.; Zhang, S.; Narasimhan, C.; Steinwender, C.; Brugada, J.; Lloyd, M.; et al. A leadless intracardiac transcatheter pacing system. *N. Engl. J. Med.* **2016**, *374*, 533−541.

(6) Jackson, N.; Olszewski, O.; O'Murchu, C.; Mathewson, A. Powering a Leadless Pacemaker Using a PiezoMEMS Energy Harvester. *Proceedings Volume 10246, Smart Sensors, Actuators, and MEMS VIII*; SPIE Microtechnologies, 2017; SPIE, 2017; DOI: 10.1117/12.2264437.

(7) Jackson, N.; Stam, F.; Olszewski, O. Z.; Doyle, H.; Quinn, A.; Mathewson, A. Widening the Bandwidth of Vibration Energy Harvesters Using a Liquid-based non-uniform Load Distribution. *Sens. Actuators, A* **2016**, *246*, 170−179.

(8) Chen, G. Z. Perception of Supercapacitor and Supercapattery. *ECS Meeting Abstracts*; The Electrochemical Society, 2011; pp 559−559.

(9) Dubal, D. P.; Ayyad, O.; Ruiz, V.; Gomez-Romero, P. Hybrid Energy Storage: the Merging of Battery and Supercapacitor Chemistries. *Chem. Soc. Rev.* **2015**, *44*, 1777−1790.

(10) Shao, H.; Padmanathan, N.; McNulty, D.; O'Dwyer, C.; Razeeb, K. M. Supercapattery Based on Binder-Free $Co_3(PO_4)_2 \cdot 8H_2O$ Multilayer Nano/Microflakes on Nickel Foam. *ACS Appl. Mater. Interfaces* **2016**, *8*, 28592−28598.

(11) Lin, T.; Chen, I.-W.; Liu, F.; Yang, C.; Bi, H.; Xu, F.; Huang, F. Nitrogen-doped Mesoporous Carbon of Extraordinary Capacitance for Electrochemical Energy Storage. *Science* **2015**, *350*, 1508−1513.
(12) Liu, S.; Zhao, Q.; Tong, M.; Zhu, X.; Wang, G.; Cai, W.; Zhang, H.; Zhao, H. Ultrafine Nickel−Cobalt Alloy Nanoparticles Incorporated into Three-dimensional Porous Graphitic Carbon as an Electrode Material for Supercapacitors. *J. Mater. Chem. A* **2016**, *4*, 17080−17086.
(13) Li, R.; Wang, Y.; Zhou, C.; Wang, C.; Ba, X.; Li, Y.; Huang, X.; Liu, J. Carbon Stabilized High capacity Ferroferric Oxide Nanorod Array for Flexible Solid state Alkaline Battery−supercapacitor Hybrid Device with High Environmental Suitability. *Adv. Funct. Mater.* **2015**, *25*, 5384−5394.
(14) He, W.; Wang, C.; Zhuge, F.; Deng, X.; Xu, X.; Zhai, T. Flexible and High Energy Density Asymmetrical Supercapacitors Based on Core/Shell Conducting Polymer Nanowires/Manganese Dioxide Nanoflakes. *Nano Energy* **2017**, *35*, 242−250.
(15) Sheberla, D.; Bachman, J. C.; Elias, J. S.; Sun, C.-J.; Shao-Horn, Y.; Dincă, M. Conductive MOF electrodes for stable supercapacitors with high areal capacitance. *Nat. Mater.* **2017**, *16*, 220−224.
(16) Leng, X.; Wu, L.; Liu, Y.; Li, C.; Wei, S.; Jiang, Z.; Wang, G.; Lian, J.; Jiang, Q. A Novel Open Architecture Built by Ultra-fine Single-crystal $Co_2(CO_3)(OH)_2$ Nanowires and Reduced Graphene Oxide for Asymmetric Supercapacitors. *J. Mater. Chem. A* **2016**, *4*, 17171−17179.
(17) Yang, J.; Yu, C.; Fan, X.; Liang, S.; Li, S.; Huang, H.; Ling, Z.; Hao, C.; Qiu, J. Electroactive Edge Site-enriched Nickel−cobalt Sulfide into Graphene Frameworks for High-performance Asymmetric Supercapacitors. *Energy Environ. Sci.* **2016**, *9* (4), 1299−1307.
(18) Yang, Y.; Cheng, D.; Chen, S.; Guan, Y.; Xiong, J. Construction of Hierarchical $NiCo_2S_4$@ $Ni(OH)_2$ Core-shell Hybrid Nanosheet Arrays on Ni Foam for High-Performance Aqueous Hybrid Supercapacitors. *Electrochim. Acta* **2016**, *193*, 116−127.
(19) Nitta, N.; Wu, F.; Lee, J. T.; Yushin, G. Li-ion Battery Materials: Present and Future. *Mater. Today* **2015**, *18*, 252−264.
(20) Li, J.; Cheng, Y.; Jia, M.; Tang, Y.; Lin, Y.; Zhang, Z.; Liu, Y. An Electrochemical−thermal Model Based on Dynamic Responses for Lithium Iron Phosphate Battery. *J. Power Sources* **2014**, *255*, 130−143.
(21) Ye, Y.; Shi, Y.; Tay, A. A. Electro-thermal Cycle Life Model for Lithium Iron Phosphate Battery. *J. Power Sources* **2012**, *217*, 509−518.
(22) Nakayama, M.; Goto, S.; Uchimoto, Y.; Wakihara, M.; Kitajima, Y. Changes in Electronic Structure Between Cobalt and Oxide Ions of Lithium Cobalt Phosphate as 4.8-V Positive Electrode Material. *Chem. Mater.* **2004**, *16*, 3399−3401.
(23) Wu, B.; Xu, H.; Mu, D.; Shi, L.; Jiang, B.; Gai, L.; Wang, L.; Liu, Q.; Ben, L.; Wu, F. Controlled Solvothermal Synthesis and Electrochemical Performance of $LiCoPO_4$ Submicron Single Crystals as a Cathode Material for Lithium Ion Batteries. *J. Power Sources* **2016**, *304*, 181−188.
(24) Kanamura, K.; Munakata, H.; Namiki, Y. Phosphate Materials for Rechargeable Battery Applications. *Phosphorus Res. Bull.* **2013**, *28*, 30−36.
(25) Tang, Y.; Liu, Z.; Guo, W.; Chen, T.; Qiao, Y.; Mu, S.; Zhao, Y.; Gao, F. Honeycomb-like Mesoporous Cobalt Nickel Phosphate Nanospheres as Novel Materials for High Performance Supercapacitor. *Electrochim. Acta* **2016**, *190*, 118−125.
(26) Bontchev, R. P.; Iliev, M. N.; Dezaneti, L. M.; Jacobson, A. J. Two New Open Framework Cobalt Phosphates: $NaCo_3(OH)(PO_4)_2.1/4H_2O$ and $Na(NH_4)Co_2(PO_4).H_2O$. *Solid State Sci.* **2001**, *3*, 133−142.
(27) Baril, M.; Assaaoudi, H.; Butler, I. S. Pressure-tuning Raman Microspectroscopic Study of Cobalt(II), Manganese(II), Zinc(II) and Magnesium(II) Pyrophosphate Dihydrates. *J. Mol. Struct.* **2005**, *751*, 168−171.
(28) Viswanathan, K.; Nayar, V.; Aruldhas, G. Infrared and Raman Spectra of Three Tetrametaphosphates $M_2P_4O_{12}$ (M = Fe, Ni, Zn). *J. Chem. Sci.* **1985**, *95*, 463−469.
(29) Chapman, A.; Thirlwell, L. Spectra of Phosphorus Compounds−I the Infra-red Spectra of Orthophosphates. *Spectrochim. Acta* **1964**, *20*, 937−947.
(30) Wang, M.; Jin, F.; Zhang, X.; Wang, J.; Huang, S.; Zhang, X.; Mu, S.; Zhao, Y.; Zhao, Y. Multihierarchical Structure of Hybridized Phosphates Anchored on Reduced Graphene Oxide for High Power Hybrid Energy Storage Devices. *ACS Sustainable Chem. Eng.* **2017**, *5*, 5679−5685.
(31) Wang, M.; Zhao, Y.; Zhang, X.; Qi, R.; Shi, S.; Li, Z.; Wang, Q.; Zhao, Y. Interface-Rich Core-shell Ammonium Nickel Cobalt Phosphate for High-performance Aqueous Hybrid Energy Storage Device without a Depressed Power Density. *Electrochim. Acta* **2018**, *272*, 184−191.
(32) Kostecki, R.; McLarnon, F. Electrochemical and in Situ Raman Spectroscopic Characterization of Nickel Hydroxide Electrodes I. Pure. Nickel Hydroxide. *J. Electrochem. Soc.* **1997**, *144*, 485−493.
(33) Preston, C. M.; Adams, W. A. A Laser Raman Spectroscopic Study of Aqueous Orthophosphate Salts. *J. Phys. Chem.* **1979**, *83*, 814−821.
(34) Tomimatsu, Y.; Kint, S.; Scherer, J. R. Resonance Raman Spectra of Iron(111)-, Copper(11)-, Cobalt(111)-, and Manganese(111)-Transferrins and of Bis(2,4,6-trichlorophenolato)-diimidazolecopper(11) Monohydrate, a Possible Model for Copper(11) Binding to Transferrins. *Biochemistry* **1976**, *15*, 4918−4924.
(35) Pang, H.; Wang, S.; Shao, W.; Zhao, S.; Yan, B.; Li, X.; Li, S.; Chen, J.; Du, W. Few-layered $CoHPO_4 \cdot 3H_2O$ Ultrathin Nanosheets for High Performance of Electrode Materials for Supercapacitors. *Nanoscale* **2013**, *5*, 5752−5757.
(36) Kissinger, P.; Heineman, W. R. *Laboratory Techniques in Electroanalytical Chemistry, Revised and Expanded*; CRC Press, 1996.
(37) Bajdich, M.; García-Mota, M.; Vojvodic, A.; Nørskov, J. K.; Bell, A. T. Theoretical Investigation of the Activity of Cobalt Oxides for the Electrochemical Oxidation of Water. *J. Am. Chem. Soc.* **2013**, *135*, 13521−13530.
(38) Kim, H.; Park, J.; Park, I.; Jin, K.; Jerng, S. E.; Kim, S. H.; Nam, K. T.; Kang, K. Coordination Tuning of Cobalt Phosphates towards Efficient Water Oxidation Catalyst. *Nat. Commun.* **2015**, *6*, 8253.
(39) Deshpande, P. P.; Sazou, D. *Corrosion Protection of Metals by Intrinsically Conducting Polymers*; CRC Press, 2016.
(40) Zanello, P. *Inorganic Electrochemistry: Theory, Practice and Application*; Royal Society of Chemistry, 2007.
(41) Akinwolemiwa, B.; Peng, C.; Chen, G. Z. Redox Electrolytes in Supercapacitors. *J. Electrochem. Soc.* **2015**, *162*, A5054−A5059.
(42) Brousse, T.; Belanger, D.; Long, J. W. To Be or Not To Be Pseudocapacitive? *J. Electrochem. Soc.* **2015**, *162*, A5185−A5189.
(43) Chen, G. Z. Understanding Supercapacitors Based on Nanohybrid Materials with Interfacial Conjugation. *Prog. Nat. Sci.* **2013**, *23*, 245−255.
(44) Padmanathan, N.; Shao, H.; McNulty, D.; O'Dwyer, C.; Razeeb, K. M. Hierarchical $NiO-In_2O_3$ Microflower (3D)/Nanorod (1D) Hetero-architecture as a Supercapattery Electrode with Excellent Cyclic Stability. *J. Mater. Chem. A* **2016**, *4*, 4820−4830.
(45) Chen, Z.; Xiong, D. B.; Zhang, X.; Ma, H.; Xia, M.; Zhao, Y. Construction of a Novel Hierarchical Structured $NH(_4)$-Co-Ni Phosphate toward an Ultrastable Aqueous Hybrid Capacitor. *Nanoscale* **2016**, *8* (12), 6636−45.
(46) Zhao, Y.; Chen, Z.; Xiong, D. B.; Qiao, Y.; Tang, Y.; Gao, F. Hybridized Phosphate with Ultrathin Nanoslices and Single Crystal Microplatelets for High Performance Supercapacitors. *Sci. Rep.* **2016**, *6*, 17613.
(47) Raju, K.; Ozoemena, K. I. Hierarchical One-Dimensional Ammonium Nickel Phosphate Microrods for High-Performance Pseudocapacitors. *Sci. Rep.* **2015**, *5*, 17629.
(48) Wang, S.; Pang, H.; Zhao, S.; Shao, W.; Zhang, N.; Zhang, J.; Chen, J.; Li, S. $NH_4CoPO_4 \cdot H_2O$ Microbundles Consisting of One-Dimensional Layered Microrods for High Performance Supercapacitors. *RSC Adv.* **2014**, *4*, 340−347.
(49) Xi, Y.; Dong, B.; Dong, Y.; Mao, N.; Ding, L.; Shi, L.; Gao, R.; Liu, W.; Su, G.; Cao, L. Well-Defined, Nanostructured, Amorphous

DOI: 10.1021/acsaem.8b01612
ACS Appl. Energy Mater. 2019, 2, 569−578

Metal Phosphate as Electrochemical Pseudocapacitor Materials with High Capacitance. *Chem. Mater.* **2016**, *28*, 1355−1362.
(50) Omar, N.; Monem, M. A.; Firouz, Y.; Salminen, J.; Smekens, J.; Hegazy, O.; Gaulous, H.; Mulder, G.; Van den Bossche, P.; Coosemans, T.; Van Mierlo, J. Lithium Iron Phosphate Based Battery−Assessment of the Aging Parameters and Development of Cycle Life Model. *Appl. Energy* **2014**, *113*, 1575−1585.
(51) Lindemark, B. Individual cell voltage equalizers (ICE) for reliable battery performance. *Proceedings*, 13th International Telecommunications Energy Conference, 1991. INTELEC '91; IEEE, 1991; pp 196−201.
(52) Lang, X.; Hirata, A.; Fujita, T.; Chen, M. Nanoporous Metal/Oxide Hybrid Electrodes for Electrochemical SupercapacitorsNat. *Nat. Nanotechnol.* **2011**, *6*, 232−236.
(53) Weng, G.-M.; Tam, L.-Y. S.; Lu, Y.-C. High-performance $LiTi_2(PO_4)_3$ Anodes for High-Areal-Capacity Flexible Aqueous Lithium-Ion Batteries. *J. Mater. Chem. A* **2017**, *5*, 11764−11771.
(54) Lai, H.; Wu, Q.; Zhao, J.; Shang, L.; Li, H.; Che, R.; Lyu, Z.; Xiong, J.; Yang, L.; Wang, X.; Hu, Z. Mesostructured NiO/Ni Composites for High-performance Electrochemical Energy Storage. *Energy Environ. Sci.* **2016**, *9*, 2053−2060.
(55) Zhang, C.; Xiao, J.; Lv, X.; Qian, L.; Yuan, S.; Wang, S.; Lei, P. Hierarchically Porous Co3O4/C Nanowire Arrays Derived from a Metal−organic Framework for High Performance Supercapacitors and the Oxygen Evolution Reaction. *J. Mater. Chem. A* **2016**, *4*, 16516−16523.
(56) Koo, M.; Park, K.-I.; Lee, S. H.; Suh, M.; Jeon, D. Y.; Choi, J. W.; Kang, K.; Lee, K. J. Bendable Inorganic Thin-film Battery for Fully Flexible Electronic Systems. *Nano Lett.* **2012**, *12*, 4810−4816.
(57) Ma, J.; Liu, W.; Zhang, S.; Ma, Z.; Song, P.; Yang, F.; Wang, X. A Thin Film Flexible Supercapacitor Based on Oblique Angle Deposited Ni/NiO Nanowire Arrays. *Nanomaterials* **2018**, *8*, 422.
(58) Pandya, S.; Wilbur, J.; Kim, J.; Gao, R.; Dasgupta, A.; Dames, C.; Martin, L. W. Pyroelectric Energy Conversion with Large Energy and Power Density in Relaxor Ferroelectric Thin Films. *Nat. Mater.* **2018**, *17*, 432−438.
(59) Conway, B. E. *Electrochemical Supercapacitors: Scientific Fundamentals and Technological Applications*; Springer Science & Business Media, 2013.
(60) Mahadevan, S. V.; Garmel, G. M. *An Introduction to Clinical Emergency Medicine*; Cambridge University Press, 2012.

DOI: 10.1021/acsaem.8b01612
ACS Appl. Energy Mater. 2019, 2, 569−578